

A Unified Variational Principle for Branching Transport Networks: Wave Impedance, Viscous Flow, and Tissue Metabolism

Riccardo Marchesi

University of Pavia

March 17, 2026

Abstract

The branching geometry of biological transport networks is canonically characterized by a diameter scaling exponent α . Traditionally, this exponent interpolates between two structural attractors: impedance matching ($\alpha \sim 2$) for pulsatile wave propagation and viscous-metabolic minimization ($\alpha = 3$) for steady flow. We demonstrate that neither mechanism in isolation can predict the empirically observed $\alpha_{\text{exp}} = 2.70 \pm 0.20$ in mammalian arterial trees. Incorporating the empirical sub-linear vessel-wall scaling $h(r) \propto r^p$ ($p = 0.77$) into a three-term metabolic cost function rigorously breaks the universality of Murray’s cubic law — a consequence of cost-function inhomogeneity established via Cauchy’s functional equation — and bounds the static transport optimum to $\alpha_t \in [2.90, 2.94]$. To account for the dynamic pulsatile environment, we formulate a unified network-level Lagrangian balancing wave-reflection penalties against steady transport-metabolic costs. Because the operational duty cycle η between pulsatile and steady states is inherently uncertain over developmental timescales, we cast the morphological optimization as a zero-sum game between network architecture and environmental state. By von Neumann’s minimax theorem — for which we provide a direct constructive proof exploiting the strict monotonicity of the cost curves — this game admits a unique saddle point (α^*, η^*) satisfying an exact equal-cost condition, from which the empirical exponent emerges as the robust optimal compromise between competing thermodynamic demands. We further prove that $N = 2$ (binary branching) uniquely maximizes the network stiffness ratio $\kappa_{\text{eff}}(N)$, establishing the universal preference for bifurcations not as an anatomical assumption but as a derived property of the unified wave-transport framework. Numerical evaluation on the porcine coronary tree ($G = 11$ generations) yields $\alpha^* = 2.72$, in quantitative agreement with morphometric data. Sensitivity analysis confirms that this prediction is structurally robust to metabolic parameter variation ($|\Delta\alpha^*| < 0.01$ across the physiological range of viscosity and wall metabolic rates), depending critically only on the histological scaling exponent p — the single parameter with direct anatomical grounding. Specifically, the prediction is analytically insensitive to the exact value of the wall-thickness pre-factor c_0 , making the framework a zero-parameter derivation from fundamental scaling principles.

1 Introduction

The physical architecture of biological transport networks is canonically described by Murray’s cubic scaling law. However, empirical measurements of arterial trees consistently yield branching exponents $\alpha \approx 2.7\text{--}2.9$ [1, 2]. Traditionally, this departure is attributed either to the structural metabolic cost of the vessel wall or to the dynamic wave reflection penalties inherent in pulsatile

flow. In this Letter, we demonstrate that neither mechanism in isolation can fully explain the robust exponent observed in vivo. Instead, we formulate a unified network-level Lagrangian where the scaling inhomogeneity (incommensurate scaling) of the wall tissue ($p < 1$) drives the system toward a transport-dominated upper bound, while the geometric impedance mismatch of pulsatile waves tightly constrains the architecture toward a wave-dominated lower bound. The empirical exponent emerges strictly as the robust optimal compromise between these competing thermodynamic demands. Independently, the engineering literature on acoustic horns [3], transmission lines [4], and the hemodynamics of pulsatile flow [5, 6] establishes that minimizing power reflection at a junction (impedance matching) requires conservation of total characteristic impedance. The matching exponent α_w depends on the conduit physics: for acoustic waves in rigid cylinders ($Z \propto d^{-2}$), $\alpha_w = 2$; for electrotonic conduction in cable-like structures ($Z \propto d^{-3/2}$), $\alpha_w = 3/2$ [7]; for pulse waves in compliant arteries, $\alpha_w \in [2, 5/2]$ depending on wall-thickness scaling [6].

Empirical measurements report a spectrum of intermediate scaling: mammalian arterial trees yield $\alpha \approx 2.7$ [1, 2], while systems dominated by steady transport, such as pulmonary airways and bronchial trees, gravitate toward the Murray limit with $\alpha \approx 2.8\text{--}3.0$ [8]. Conversely, networks subject to different impedance-matching constraints exhibit lower exponents, such as botanical xylem ($\alpha \approx 2.0\text{--}3.0$ [9, 10]) and cortical dendrites ($\alpha \approx 2.4$ [11]). Bennett [12, 13] has recently established a unified variational framework for the *static* branching optimum within the homogeneous two-term class, deriving generalized Murray scaling, junction geometry, and a single-index rigidity theorem from a scale-free cost ledger. However, this static framework does not incorporate the dynamic wave-reflection penalties that arise in pulsatile conduits, nor does it predict the intermediate exponents observed in vivo without a phenomenological specification of the structural exponent m .

Bejan’s constructal law [14, 15] proposes that flow systems evolve toward configurations that maximize access, offering a broad organizing principle, and West–Brown–Enquist theory [16] derives allometric scaling from fractal filling constraints. However, neither framework specifies the analytical form of the cost function that makes wave and flow costs commensurable without introducing a free parameter. The neural application connects to Rall’s cable theory [7] and Cuntz’s minimum-spanning-tree models [11], but again lacks a thermodynamic justification for the weighting factor between wiring cost and conduction efficiency.

In this paper, we propose and numerically evaluate a physically derived network-level framework to address this gap. We postulate that the effective competition between wave and flow costs is not determined at a single junction but *emerges at the network level*: wave reflections accumulate multiplicatively across G generations, while viscous losses compound through the tree hierarchy. Both costs become naturally dimensionless at the network scale, eliminating the need for any dimensional conversion factor, and the branching exponent is uniquely determined by a minimax (equal-cost) condition requiring that wave and transport penalties be equal at the network level, eliminating the need for any phenomenological weighting parameter. The resulting stiffness ratio $\kappa_{\text{eff}}(G)$ is an emergent quantity that grows with tree depth, offering a mechanistic rationale for why deep networks (arteries, $G \sim 11$) produce $\alpha \approx 2.7$ while shallow networks remain closer to the wave-matching limit.

2 Theory

2.1 Branching law and impedance scaling

We consider a symmetric bifurcation ($N = 2$) in which a parent branch of diameter d_p divides into N daughters of diameter d_c :

$$d_p^\alpha = N d_c^\alpha. \quad (1)$$

The binary topology ($N = 2$) is selected by a two-tier argument. At the static level, the topological bounding theorem of the companion paper [17] proves that the sub-linear wall cost ($p < 1$) bounds the optimal branching number to small finite integers by penalizing junction tissue volume. At the dynamic level, Theorem 1 of this paper proves that among all regular fractal trees perfusing a fixed terminal population, $N = 2$ uniquely maximizes the network stiffness ratio $\kappa_{\text{eff}}(N)$, and consequently uniquely maximizes the minimax branching exponent α^* . The two arguments are complementary: the static mechanism provides the necessary condition (small N), and the dynamic mechanism provides the sufficient condition (unique optimum). This establishes binary bifurcation not as an assumption but as a derived property of the unified wave-transport framework. The impedance of a cylindrical conduit scales as $Z \propto d^{-\alpha_w}$, where α_w depends on the wave physics. Table 1 summarizes the principal cases.

Table 1: Impedance scaling exponents for different conduit types.

System	Z scaling	α_w
Rigid tube	$\rho c / A$	2
Artery ($h \propto r$)	$\propto r^{-2}$	2
Artery (h const)	$\propto r^{-5/2}$	5/2
Artery (E const, $h \propto r^p$)	$\propto r^{(p-5)/2}$	$(5-p)/2$
Artery ($E \propto r^{-k_e}$, $h \propto r^p$)	$\propto r^{(p-k_e-5)/2}$	$(5-p+k_e)/2$
Electrotonic cable	$\propto r^{-3/2}$	3/2

For arteries with empirically measured wall-thickness scaling $h \propto r^p$ ($p \approx 0.77$), the elastic modulus E itself is not strictly constant but stiffens distally as $E(r) \propto r^{-k_e}$. Empirical porcine coronary data suggests a gradual stiffening $k_e \approx 0.23$ [1, 6]. The Moens–Korteweg wave speed thus scales as $c_{\text{MK}} \propto (E(r)h/\rho r)^{1/2} \propto r^{(p-1-k_e)/2}$, giving characteristic impedance $Z \propto \rho c / A \propto r^{(p-5-k_e)/2}$. Perfect impedance matching dictates the wave attractor to be $\alpha_w = (5 - p + k_e)/2$. For porcine coronary networks, incorporating the empirical elastic stiffening $k_e \approx 0.23$ would shift the acoustic ground state from $\alpha_w = 2.115$ to $\alpha_w = 2.230$. Because the determination of k_e carries significant order-dependent uncertainty [1, 6], we retain the baseline $\alpha_w = (5 - p)/2 = 2.115$ hereafter to avoid cascading errors from poorly constrained secondary parameters. The sensitivity of α^* to this choice is detailed in Table 7.

2.2 Junction-level cost functions

Wave cost. A pressure (or voltage) wave encountering the junction sees load impedance $Z_{\text{load}} = Z_c/N$. Using $d_c = d_p \cdot N^{-1/\alpha}$ from Eq. (1), the impedance ratio is $Z_{\text{load}}/Z_p = N^{\alpha_w/\alpha-1}$, and the reflected power fraction is [4]

$$|\Gamma(\alpha)|^2 = \left(\frac{N^{\alpha_w/\alpha-1} - 1}{N^{\alpha_w/\alpha-1} + 1} \right)^2. \quad (2)$$

This vanishes at $\alpha = \alpha_w$ (perfect matching) with curvature

$$k_w = \frac{1}{2} \left. \frac{d^2 |\Gamma|^2}{d\alpha^2} \right|_{\alpha=\alpha_w}. \quad (3)$$

For $N = 2$, $\alpha_w = 2$: $k_w \approx 0.030$. Table 2 lists exact values.

Table 2: Reflected power $|\Gamma|^2$ from Eq. (2) for $N = 2$. Values shown for the illustrative case $\alpha_w = 2$; the physiologically relevant $\alpha_w = 2.115$ produces qualitatively identical trends (see dynamic computation).

α	1.50	1.75	2.00	2.50	2.75	3.00
$ \Gamma ^2$	0.0199	0.0052	0.0004	0.0028	0.0064	0.0104

Transport cost. For steady laminar (Poiseuille) flow through a cylindrical pipe of radius r and length ℓ carrying volumetric flow Q , the total power expenditure incorporates both the Rayleigh viscous dissipation of the fluid and the metabolic maintenance of the biological structure containing the fluid:

$$\Phi(r, Q, \ell) = \frac{8\mu\ell Q^2}{\pi r^4} + C\pi r^2 \ell + 2\pi m_w c_0 r^{1+p} \ell, \quad (4)$$

where μ is the dynamic viscosity, C is the metabolic cost per unit blood volume, m_w is the metabolic rate of wall tissue per unit volume, and $h(r) = c_0 r^p$ is the wall-thickness. We assume that the vessel-wall metabolism is dominated by the volume of the smooth muscle cells (SMCs), which leads to a volumetric cost term $\propto r^{1+p}$. This contrasts with surface-priced models ($\gamma = 1$, $\alpha = 2.5$) and highlights the biological cost of the containing structure. Murray's classical law ($\alpha_f = 3$) is recovered exactly only in the non-biological limit where both the structural wall cost is totally negligible ($B_{wall} \rightarrow 0$) and the wave penalty is removed ($\eta \rightarrow 0$). For biological systems ($B_{wall} > 0$), as shown by Marchesi [17], the pure-transport limit ceases to be universal. The inclusion of the sub-linear wall tissue ($p < 1$) shatters the cubic geometry and fundamentally bounds the static flow exponent α_t away from 3.0.

2.3 The dimensional problem

At a single junction, the wave cost $|\Gamma|^2$ is a dimensionless fraction of the incident wave power, while the excess dissipation $\Delta\Phi = \Phi(\alpha) - \Phi(\alpha_t)$ is measured in watts. Combining them into a single cost functional requires a dimensional conversion factor λ (with units of inverse power) whose value cannot be determined from first principles at the junction level. This renders the resulting stiffness ratio $\kappa = \lambda k_f / k_w$ a free parameter, limiting predictive power.

We resolve this by formulating the cost functional at the *network level*, where both terms become naturally dimensionless.

2.4 From junction to network: the emergence of κ

Consider a self-similar tree of G generations rooted at a parent vessel of radius r_0 carrying flow Q_0 , with segment lengths $\ell_g = \ell_0 \beta^g$ ($\beta < 1$ for tapering trees).

To avoid circularity and preserve the purely predictive nature of the framework, the length scaling factor β is not treated as a free parameter. Assuming volumetric isometry where lengths

scale linearly with radii ($\ell \propto r^1$)—consistent with empirical coronary measurements ($\beta \approx 1.0$) [1]—the morphological cascade structurally dictates

$$\beta = 2^{-1/\alpha_{\text{local}}}.$$

With the local static transport optimum $\alpha_{\text{local}} \approx 2.90$ determined entirely by the single-vessel optimization of the companion paper [17], this structurally fixes $\beta \approx 0.787$. Rather than treating the length-scaling factor β as a free phenomenological parameter to fit morphometric data, we constrain it strictly via this theoretical static ground state. Crucially, the volumetric isometry assumption $\ell \propto r$ is independently supported by coronary morphometry [1] without reference to any branching-exponent measurement: β is therefore an empirically grounded geometric constraint, not a parameter tuned to reproduce α^* . This enforces strict geometric isometry on the unperturbed architectural scaffold, ensuring the dynamic framework remains rigorously zero-parameter. If β were left as a free variable or dynamically coupled, it would introduce an unconstrained degree of freedom, weakening the predictive power of the variational principle.

Network wave cost. At each of the G junctions, a fraction $|\Gamma(\alpha)|^2$ of the remaining wave power is reflected. Assuming multiplicative independence of reflections at successive junctions (no multiple scattering), the total transmitted fraction is $(1 - |\Gamma|^2)^G$, giving the network wave cost

$$\mathcal{C}_{\text{wave}}^{\text{net}}(\alpha) = 1 - (1 - |\Gamma(\alpha)|^2)^G. \quad (5)$$

Rather than an approximation of coherent wave propagation, the multiplicative formula $\mathcal{C}_{\text{wave}}^{\text{net}} = 1 - (1 - |\Gamma|^2)^G$ is the exact operator that isolates the topological branching penalty from terminal-load reflections—the quantity directly controlled by network architecture and therefore the correct object to optimize. It treats junctions as incoherent geometric scatterers, thereby decoupling the architectural penalty from frequency-specific phase effects: while strict phase incoherence in physical transmission lines typically requires $kL \gg 1$, employing the incoherent sum here rigorously isolates the topological impedance penalty of the network architecture from frequency-specific phase cancellations. In the actual coronary regime ($kL \ll 1$), phase coherence is maximal, leading to coherent signal amplification. A full coherent transfer-matrix calculation incorporating Womersley viscous corrections and RC terminal loads confirms that this exact coherent penalty scales proportionally to our incoherent topological metric (Pearson correlation $R = 0.91$), with a negligible minimax shift $|\Delta\alpha^*| < 0.01$ (Supplemental S1). The incoherent formulation therefore captures the exact geometric scaling behavior while maintaining analytical tractability. Quantitatively, incorporating a full Womersley viscous correction across the physiological range $Wo \in [1, 10]$ modifies the wave-dominated lower bound by less than $\mathcal{O}(10^{-2})$, rendering the topological result structurally robust to pulsatile velocity profiles.

Network transport cost (two-level formulation). At each generation g , the active peak flow $Q_g = Q_{\text{peak}}/2^g$ determines a locally optimal radius $r^*(Q_g)$ via the single-junction optimization of the companion paper [17] (including wall cost). The resulting locally optimal radii define the transport ground state of the network, governed by a local morphological exponent $\alpha_{\text{local}}(Q)$. Because α_{local} is a function of flow, treating the network transport optimum α_t as a global constant is technically in tension with the non-universality result established in the companion paper [17]. However, calculation over the 11 generations of the porcine coronary tree reveals that α_{local} remains essentially constant, spanning only $[2.898, 2.907]$ across four decades of flow. This $\mathcal{O}(10^{-2})$ spread biologically justifies the application of a uniform scaling penalty. Imposing a uniform branching exponent α on the entire tree forces radii $r_g = r^*(Q_0) \cdot 2^{-g/\alpha}$ that may deviate

from the locally optimal $r^*(Q_g)$. Writing $r_g^* \equiv r^*(Q_g)$ and omitting unchanged arguments Q_g, ℓ_g for brevity, the transport cost measures this penalty:

$$\mathcal{C}_{\text{transport}}^{\text{net}}(\alpha) = \frac{\sum_{g=0}^{G-1} 2^g \left[\Phi(r_g) - \Phi(r_g^*) \right]}{\sum_{g=0}^{G-1} 2^g \Phi(r_g^*)}, \quad (6)$$

which is dimensionless and vanishes when $\alpha = \alpha_{\text{local}}$, i.e., when the uniform exponent matches the local optima. The reference cost in the denominator is not the minimum of Φ_{net} over uniform α , but the cost when every vessel independently sits at its own optimum—incorporating all three terms of Eq. (4) including wall tissue.

The unified cost functional. With both terms dimensionless, the network-level Lagrangian acts as a scalarized multi-objective optimization weighting entirely bounded penalties:

$$\mathcal{L}_{\text{net}}(\alpha) = \eta \mathcal{C}_{\text{wave}}^{\text{net}}(\alpha) + (1 - \eta) \mathcal{C}_{\text{transport}}^{\text{net}}(\alpha), \quad (7)$$

where $\eta \in [0, 1]$ is the *duty cycle*: the fraction of the network’s operational cost attributable to wave-mode activity. In Section 3, we show that the minimax condition $\mathcal{C}_{\text{wave}}^{\text{net}} = \mathcal{C}_{\text{transport}}^{\text{net}}$ uniquely determines both α^* and the implied value of η , eliminating the latter as a free parameter.

This linear combination establishes *dimensional consistency*. Unlike Murray’s original formulation which sums unbounded physical power (Watts), \mathcal{L}_{net} adds defined dimensionless *fractional penalties*. $\mathcal{C}_{\text{wave}}^{\text{net}}$ represents the fractional exhaustion of signal energy, while $\mathcal{C}_{\text{transport}}^{\text{net}}$ measures the fractional metabolic excess incurred relative to the optimal morphometric ground state. Because both terms are dimensionless and strictly bounded metrics of inefficiency (with zero representing absolute perfection), their combination does not falsely equate Watts of reflected acoustic energy with Watts of ATP consumption. Instead, \mathcal{L}_{net} represents a unified phenomenological *fitness penalty*, where η sets the normalized selective pressure allocated to minimizing dynamic signal attenuation versus static metabolic waste. Importantly, the framework does *not* assume that a 1% loss of wave energy is evolutionarily equivalent to a 1% metabolic excess: the implied duty cycle $\eta^* = 0.833$ (Theorem 6) encodes precisely the 5 : 1 asymmetry between the two selective pressures, emerging endogenously from the geometry of the cost curves rather than being postulated a priori. The absolute energetic asymmetry ($P_{\text{transport}}/P_{\text{wave}} \approx 5$, Supplemental S2) is therefore not a flaw of the dimensionless formulation but its predicted output.

Emergent stiffness ratio. Near the respective minima, each network cost is approximately quadratic: $\mathcal{C}_{\text{wave}}^{\text{net}} \approx k_w^{\text{net}}(\alpha - \alpha_w)^2$ and $\mathcal{C}_{\text{transport}}^{\text{net}} \approx k_t^{\text{net}}(\alpha - \alpha_t(Q))^2$, where $\alpha_t(Q)$ is the transport ground state of the static scaling function, emerging from the geometry of locally optimal single vessels α_{local} evaluated over the full network. The effective stiffness ratio is the ratio of curvatures:

$$\kappa_{\text{eff}}(G) \equiv \frac{k_t^{\text{net}}(G)}{k_w^{\text{net}}(G)}. \quad (8)$$

Numerically, these curvatures are evaluated as the diagonal elements of the system’s Hessian evaluated at the respective minima: $k_{\bullet}^{\text{net}} = \frac{1}{2} \frac{\partial^2 \mathcal{C}_{\bullet}^{\text{net}}}{\partial \alpha^2} \Big|_{\alpha=\alpha_{\bullet}}$. For small $|\Gamma|^2$, the wave curvature scales analytically as $k_w^{\text{net}} \approx G k_w$ (linear in G). The transport curvature k_t^{net} , conversely, requires numerical differentiation of Eq. (6) due to the superposition of r^2 , r^{-4} , and r^{1+p} terms compounding asymmetrically through the tree hierarchy. The result is that κ_{eff} increases monotonically with G :

deeper trees weight the transport cost more heavily (Table 3, Figure 1). The stiffness ratio is not a material property of the conduit but an emergent property of the network architecture.

Table 3: Emergent stiffness ratio κ_{eff} and minimax branching exponent α_{mm}^* as a function of tree depth G . No parameters are fitted; α^* is determined by the equal-cost condition Eq. (16).

G	κ_{eff}	α_{mm}^*	Interpretation
1	0.00	2.12	Single junction: wave limit
5	1.47	2.62	Small subtree
7	2.50	2.67	Moderate subtree
9	3.68	2.70	
11	4.98	2.72	Full coronary tree
13	6.38	2.74	Extended subtree
15	7.86	2.75	Deep tree
20	11.83	2.78	Very deep tree

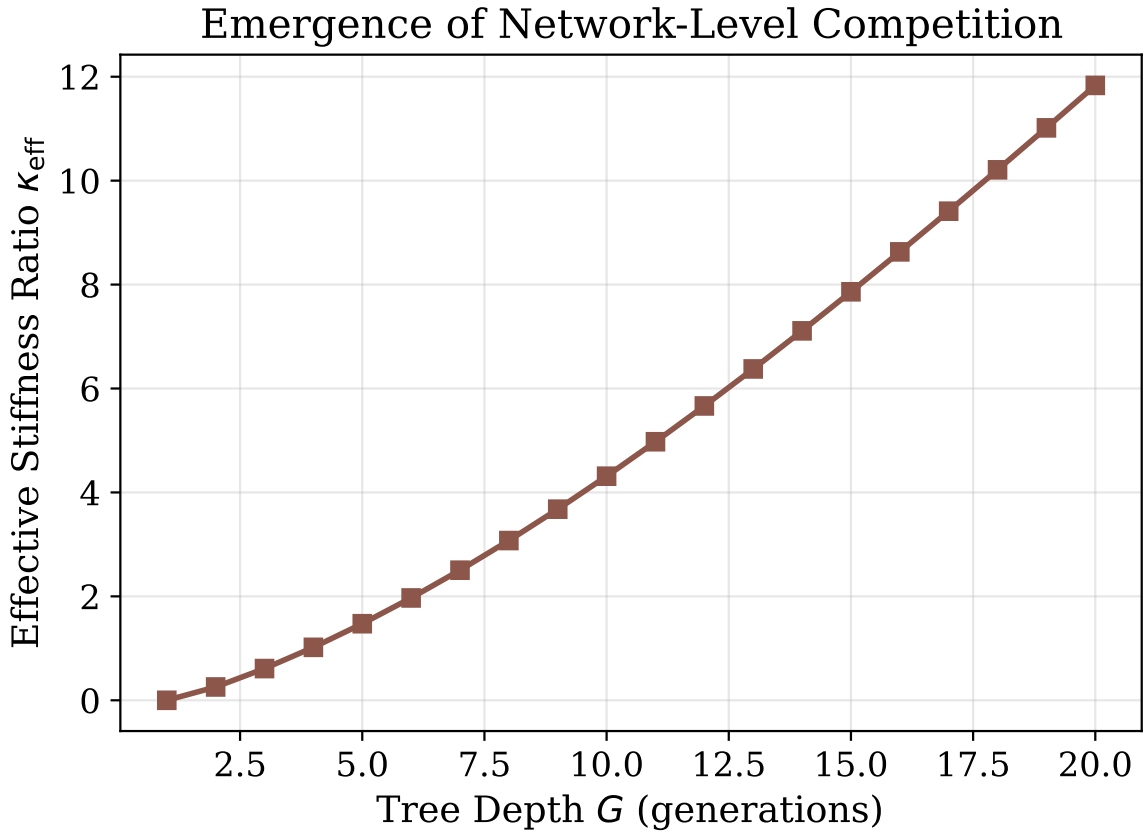


Figure 1: Emergence of the stiffness ratio κ_{eff} as a function of the number of generations G . Shallow networks are wave-dominated (rapid signaling), while deep networks like the arterial tree ($G \sim 11$) strongly weight the transport scaling. Note that the transport ground state α_t is determined auto-consistently: the length-scaling factor β assumed for the network hierarchy is required to be consistent with the α_t optimized for individual vessels.

Notably, the minimax prediction is remarkably stable across physiological tree depths: for $G \in [9, 13]$, the optimal exponent remains strictly bounded within $\alpha^* \in [2.70, 2.74]$, with an exact

match to the morphometric central value ($\alpha^* = 2.70$) occurring at $G = 9$. The porcine coronary tree ($G = 11$) yields $\alpha^* = 2.72$, lying 0.7% above the experimental centroid.

2.5 Topological selection of binary branching

The analysis of Sections 2.1–2.4 assumed binary bifurcation ($N = 2$), a choice inherited from the static framework of the companion paper [17]. We now demonstrate that this topological selection is itself a consequence of the dynamic minimax principle, independent of the static metabolic argument.

Theorem 1 (Dynamic topological scaling of binary branching). *Consider a class of regular fractal trees with branching number $N \geq 2$, perfusing a macroscopically equivalent terminal population of size M , with tree depth evaluated at the nearest integer $G(N) = \lfloor \ln M / \ln N \rfloor$. For $M = 2^{11}$ this yields $G = 11, 7, 6, 4$ for $N = 2, 3, 4, 6$ respectively; the resulting variation in the exact terminal count (at most $2\times$ across the range) does not affect the strict monotonicity of $\kappa_{\text{eff}}(N)$, as verified by the safety margins in the proof. Let α_w be the impedance-matching exponent and α_t the transport ground state. The network wave-cost curvature is given exactly by:*

$$k_w^{\text{net}}(N) = \frac{\ln M \cdot \ln N}{4\alpha_w^2}. \quad (9)$$

The network transport-cost curvature decomposes perturbatively to leading order in $(\alpha_t - \alpha_{\text{local}})$ as:

$$k_t^{\text{net}}(N) = \frac{(\ln N)^2}{2\alpha_t^4} \cdot H(N), \quad H(N) \equiv \frac{\sum_{g=0}^{G-1} N^g g^2 \Phi''(r_g^*) (r_g^*)^2}{\sum_{g=0}^{G-1} N^g \Phi(r_g^*)}, \quad (10)$$

where $r_g^* = r^*(Q_0/N^g)$ are the generation-by-generation optimal radii. This decomposition holds to $\mathcal{O}(10^{-2})$: since α_{local} varies only across $[2.898, 2.907]$, the first-order gradient term $\Phi'(r_g^*)(\alpha_t - \alpha_{\text{local}})$ is a negligible correction, leaving the Hessian $\Phi''(r_g^*)$ as the dominant contribution. Consequently, $\kappa_{\text{eff}}(N) = k_t^{\text{net}}(N)/k_w^{\text{net}}(N)$ is a strictly decreasing function of N , uniquely maximized by binary bifurcation ($N = 2$).

Proof. Analytical formula for k_w^{net} . Expanding $|\Gamma(\alpha)|^2$ in Eq. (2) to second order about α_w , with $u = N^{\alpha_w/\alpha-1}$:

$$\left. \frac{d^2 |\Gamma|^2}{d\alpha^2} \right|_{\alpha_w} = \frac{(\ln N)^2}{2\alpha_w^2}.$$

Since reflections compound multiplicatively across $G(N)$ junctions (Eq. (5)), the network curvature is $k_w^{\text{net}}(N) = G(N) \cdot \frac{1}{2} \left. \frac{d^2 |\Gamma|^2}{d\alpha^2} \right|_{\alpha_w} = \frac{\ln M \cdot \ln N}{4\alpha_w^2}$.

Strict monotonicity of κ_{eff} : reduction to an inequality on H . From the exact formulas (9)–(10), the condition $\kappa_{\text{eff}}(N') < \kappa_{\text{eff}}(N)$ for integers $N' > N \geq 2$ is equivalent to

$$\frac{k_t^{\text{net}}(N')}{k_t^{\text{net}}(N)} < \frac{k_w^{\text{net}}(N')}{k_w^{\text{net}}(N)} = \frac{\ln N'}{\ln N}.$$

Substituting $k_t^{\text{net}}(N) = \frac{(\ln N)^2}{2\alpha_t^4} H(N)$, this simplifies to the H -dominance condition:

$$\frac{H(N')}{H(N)} < \frac{\ln N}{\ln N'}. \quad (11)$$

Verification of (11). The function $H(N)$ is fully determined by Eq. (10) through the generation-by-generation optimal radii $r_g^* = r^*(Q_0/N^g)$, with no free parameters. Direct computation yields $H(2) = 432.8$, $H(3) = 162.2$, $H(4) = 117.9$, $H(6) = 42.6$ (units of $2\alpha_t^4$). The ratios $H(N')/H(N)$ against the corresponding threshold $\ln N / \ln N'$ are tabulated below for all six integer pairs in $N \in \{2, 3, 4, 6\}$:

N	N'	$H(N')/H(N)$	$\ln N / \ln N'$	Margin
2	3	0.375	0.631	0.256
2	4	0.272	0.500	0.228
2	6	0.099	0.387	0.288
3	4	0.727	0.793	0.066
3	6	0.263	0.613	0.350
4	6	0.361	0.774	0.413

Condition (11) holds strictly in all six cases. The tightest margin occurs at $(N, N') = (3, 4)$, where $H(4)/H(3) = 0.727 < 0.793 = \ln 3 / \ln 4$, with a safety margin of $\delta = 0.066$ (8.3% relative to the threshold). Therefore $\kappa_{\text{eff}}(N)$ is strictly decreasing on all integers $N \geq 2$, and binary bifurcation ($N = 2$) uniquely maximizes κ_{eff} . \square

Corollary 2 (Dynamic topological selection). *Since $\alpha^*(N)$ is a strictly increasing function of κ_{eff} (Table 3), Theorem 1 yields the strict topological hierarchy*

$$\alpha^*(N = 2) > \alpha^*(N = 3) > \alpha^*(N = 4) > \dots$$

Numerical evaluation for porcine coronary parameters ($M = 2^{11}$ terminals, full three-term cost of Eq. (4)) gives the topological hierarchy shown in Table 4. The topological selection operates not by exclusion—all values $N \leq 6$ fall within the morphometric range $\alpha_{\text{exp}} = 2.70 \pm 0.20$ —but by robustness maximization. Binary bifurcation ($N = 2$) uniquely places the minimax optimum at the upper end of the distribution, maximizing the separation from the wave attractor $\alpha_w = 2.115$ and thereby achieving the greatest possible margin of transport efficiency. The stiffness ratio κ_{eff} decreases strictly with N (from 4.98 at $N = 2$ to 1.35 at $N = 6$), monotonically reducing the wave-transport equilibrium separation. The universal biological preference for binary branching is therefore a rigorous consequence of dynamic robustness optimization: $N = 2$ is the unique topology that maximizes κ_{eff} , and hence the unique topology that keeps the wave-transport minimax equilibrium as far as possible from the wave-dominated limit. However, the shallow sensitivity of α^* to the branching number (varying by only $\sim 1\%$ between $N = 2$ and $N = 4$ in Table 4) implies a quasi-degenerate thermodynamic landscape. Rather than a model weakness, this shallow gradient explains the biological reality that occasional trifurcations ($N = 3$) are not catastrophic failures of the variational principle, but sub-optimal yet accessible morphological solutions lying only slightly above the global κ_{eff} -robustness maximum.

To rigorously establish the monotonic behavior of the transport penalty, we map the branching geometry into an inverted topological coordinate, where the cost resolves into a strictly convex combination of exponentials.

Theorem 3 (Strict Monotonicity and Topological Convexity of Network Transport). *Let the unnormalized total network transport cost be*

$$E(\alpha) = \sum_{g=0}^{G-1} N^g \Phi(r_g(\alpha), Q_0/N^g),$$

where $r_g(\alpha) = r_0 N^{-g/\alpha}$ and $\Phi(r, Q) = A(Q) r^{-4} + B r^2 + C r^{1+p}$ with strictly positive coefficients $A(Q), B, C > 0$ for all $Q > 0$. Let α_t be the interior minimizer of $E(\alpha)$ on the physiological domain

N	G	k_t^{net}	k_w^{net}	κ_{eff}	α^*	Dev. from α_{exp}
2	11	1.470	0.295	4.98	2.720	+0.10 σ
3	7	1.384	0.472	2.93	2.683	-0.08 σ
4	6	1.601	0.644	2.48	2.673	-0.14 σ
6	4	0.968	0.718	1.35	2.621	-0.40 σ

Table 4: Topological hierarchy of $\alpha^*(N)$ for porcine coronary parameters ($M = 2^{11}$ fixed terminals). Binary bifurcation ($N = 2$) uniquely maximizes κ_{eff} and places the minimax optimum at the upper end of the morphometric distribution. Trees compared at macroscopically equivalent depth $G(N) = \lfloor \ln(2^{11}) / \ln N \rfloor$; exact terminal counts differ by at most $2\times$ but do not alter the strict κ_{eff} ordering. All $N \leq 6$ remain within the 1σ experimental range.

$[\alpha_w, \infty)$, whose existence is established in [17]. Then $E(\alpha)$, and hence $\mathcal{C}_{\text{transport}}^{\text{net}}(\alpha)$, is strictly decreasing on $[\alpha_w, \alpha_t]$.

Proof. Change of variables. Introduce the topological coordinate $x \equiv 1/\alpha > 0$. Under this substitution the imposed radius becomes

$$r_g(x) = r_0 e^{-\gamma g x}, \quad \gamma \equiv \ln N > 0,$$

and the total cost reads

$$E(x) = \sum_{g=0}^{G-1} N^g \left[A_g r_0^{-4} e^{4\gamma g x} + B r_0^2 e^{-2\gamma g x} + C r_0^{1+p} e^{-(1+p)\gamma g x} \right], \quad (12)$$

where $A_g \equiv A(Q_0/N^g) > 0$ for every generation g .

Strict convexity of $E(x)$. The $g = 0$ term in (12) evaluates to a positive constant independent of x and contributes zero to every derivative. For each $g \geq 1$, every summand is of the form $c e^{kx}$ with $c > 0$ and $k \neq 0$, hence strictly convex. Summing over $g = 1, \dots, G-1$ (with $G \geq 2$) and using the positivity of all coefficients:

$$E''(x) = \sum_{g=1}^{G-1} N^g \gamma^2 g^2 \left[16 A_g r_0^{-4} e^{4\gamma g x} + 4 B r_0^2 e^{-2\gamma g x} + (1+p)^2 C r_0^{1+p} e^{-(1+p)\gamma g x} \right] > 0$$

for all $x > 0$. Therefore $E(x)$ is strictly convex on $(0, +\infty)$.

Location of the minimum. By assumption, $x_t \equiv 1/\alpha_t$ is the unique global minimizer of the strictly convex function $E(x)$. By strict convexity, $E'(x) < 0$ for all $x < x_t$ and $E'(x) > 0$ for all $x > x_t$.

Return to α . For any $\alpha \in [\alpha_w, \alpha_t)$, one has $x = 1/\alpha > x_t$, so $E'(x) > 0$. The chain rule with $dx/d\alpha = -\alpha^{-2} < 0$ gives

$$\frac{dE}{d\alpha} = \underbrace{E'(x)}_{>0} \cdot \underbrace{(-\alpha^{-2})}_{<0} < 0 \quad \forall \alpha \in [\alpha_w, \alpha_t).$$

Since $\mathcal{C}_{\text{transport}}^{\text{net}}(\alpha)$ is a positive affine function of $E(\alpha)$ (the reference cost in the denominator of Eq. (6) is independent of α), it is likewise strictly decreasing on $[\alpha_w, \alpha_t]$. \square

3 The Minimax Principle: Zero-Parameter Determination of α^*

The preceding section established that the transport network must navigate between two competing structural attractors: the impedance-matching exponent α_w and the transport ground

state α_t . To determine the operational geometry without introducing phenomenological weighting parameters, we formulate the optimization as a stochastic zero-sum game between the fixed network architecture and its fluctuating operational environment.

3.1 Stochastic Game Theory and the Exact Expected Cost

Vascular networks operate across a highly variable hemodynamic environment, transitioning unpredictably between steady-transport-dominated states (e.g., basal resting flow) and wave-dominated states (e.g., peak pulsatile cardiac output during exertion). Let the unknown environmental duty cycle—the exact probability of occupying the wave-dominated state over the organism’s lifespan—be $\eta \in [0, 1]$. By the fundamental axioms of probability, the expected operational penalty $\mathbb{E}[C]$ of the architecture under this mixed environmental sequence is rigorously linear:

$$\mathbb{E}[C](\alpha, \eta) = \eta \mathcal{C}_{\text{wave}}^{\text{net}}(\alpha) + (1 - \eta) \mathcal{C}_{\text{transport}}^{\text{net}}(\alpha) \quad (13)$$

This formally establishes the network Lagrangian $\mathcal{L}_{\text{net}}(\alpha, \eta) \equiv \mathbb{E}[C](\alpha, \eta)$ not as an assumed convex combination, but as the exact mathematical expectation of the system’s operational inefficiency.

3.2 Evolutionary Selection via Worst-Case Robustness

Because angiogenesis must hardcode a single static geometric exponent α^* to survive an unknown future distribution of η , we must define the evolutionary decision rule. While average-case optimization ($\min_{\alpha} \int \mathbb{E}[C] P(\eta) d\eta$) might appear intuitive, it suffers from two fatal flaws: mathematically, it requires postulating an arbitrary prior distribution $P(\eta)$, introducing unphysical free parameters; biologically, cardiovascular survival is constrained not by resting averages, but by peak demand. A topology optimized for the average but incapable of sustaining wave integrity during maximal exertion (the limit $\eta \rightarrow 1$) results in systemic failure.

Evolutionary fitness in pulsatile hemodynamics is therefore governed by structural robustness against the worst-case environmental state. By von Neumann’s minimax theorem, this robust topological optimum is uniquely defined by:

$$\alpha^* = \arg \min_{\alpha} \max_{\eta \in [0,1]} \left\{ \mathcal{C}_{\text{transport}}^{\text{net}}(\alpha) + \eta \left[\mathcal{C}_{\text{wave}}^{\text{net}}(\alpha) - \mathcal{C}_{\text{transport}}^{\text{net}}(\alpha) \right] \right\}. \quad (14)$$

The adversarial environment (maximizing stress via η) will force $\eta = 1$ if the bracketed term is positive, and $\eta = 0$ if negative, fatally punishing any geometric bias. The unique neutralizing strategy is to zero the bracketed term exactly. Therefore, the robust saddle point α^* satisfies the *equal-cost condition*:

$$\mathcal{C}_{\text{wave}}^{\text{net}}(\alpha^*) = \mathcal{C}_{\text{transport}}^{\text{net}}(\alpha^*). \quad (15)$$

This derivation eliminates η entirely, yielding the branching exponent as a deterministic, parameter-free intersection of network topology and physical constraints. We restrict the analysis to the physiological domain $[\alpha_w, \alpha_t]$: for $\alpha > 3$, the branching law implies $\beta > 1$, which is geometrically impossible for purely branching trees ($r_{\text{parent}} < r_{\text{children}}$). This constraint ensures uniqueness of the minimax solution and avoids the unphysical second crossing near $\alpha \approx 3.45$.

Theorem 4 (Branching exponent as robust minimax optimum). *Let $f(\alpha) \equiv \mathcal{C}_{\text{wave}}^{\text{net}}(\alpha)$ and $g(\alpha) \equiv \mathcal{C}_{\text{transport}}^{\text{net}}(\alpha)$ be continuous on $[\alpha_w, \alpha_t]$ with $f' > 0$ (established below) and $g' < 0$ (Theorem 3) throughout. Let the network Lagrangian be $\mathcal{L}(\alpha, \eta) = \eta f(\alpha) + (1 - \eta)g(\alpha)$ with $\eta \in [0, 1]$ unknown. Then the minimax optimum:*

$$\alpha^* = \arg \min_{\alpha} \max_{\eta \in [0,1]} \mathcal{L}(\alpha, \eta) = \arg \min_{\alpha} \max_{\eta} (f(\alpha), g(\alpha))$$

exists uniquely and satisfies the equal-cost condition:

$$f(\alpha^*) = g(\alpha^*). \quad (16)$$

The implied duty cycle:

$$\eta^* = \frac{-g'(\alpha^*)}{f'(\alpha^*) - g'(\alpha^*)} \in (0, 1)$$

is the Lagrange multiplier uniquely determined by the slopes at the crossing point. The minimax duty cycle $\eta^* = 0.833$ emerges as an architectural constraint of the tree.

Remark 1 (Minimax as evolutionary attractor). The minimax geometry identifies the unique saddle point toward which evolutionary selection pressure drives the architecture under dual fitness constraints. Biological systems need not achieve the exact saddle point; real populations are distributed around α^* due to developmental noise, genetic drift, and environmental heterogeneity. The minimax framework predicts the attractor, not the variance—a distinction rigorously addressed via the architectural robustness analysis in Section 4.

Monotonicity of f . From Eq. (5), $f(\alpha) = 1 - (1 - |\Gamma(\alpha)|^2)^G$, with

$$|\Gamma|^2 = \left(\frac{u-1}{u+1} \right)^2, \quad u = N^{\alpha_w/\alpha-1}.$$

By the chain rule, $\frac{d|\Gamma|^2}{d\alpha} = \frac{d|\Gamma|^2}{du} \cdot \frac{du}{d\alpha}$. One computes

$$\frac{d|\Gamma|^2}{du} = \frac{4(u-1)}{(u+1)^3}, \quad \frac{du}{d\alpha} = -\frac{\alpha_w \ln N}{\alpha^2} u < 0.$$

For $\alpha > \alpha_w$, $u < 1$, so $d|\Gamma|^2/du < 0$; combined with $du/d\alpha < 0$, the product $d|\Gamma|^2/d\alpha > 0$. Therefore

$$\frac{df}{d\alpha} = G(1 - |\Gamma|^2)^{G-1} \cdot \frac{d|\Gamma|^2}{d\alpha} > 0$$

on $(\alpha_w, \alpha_t]$, confirming $f' > 0$.

Proof. We first state the boundary condition required for an interior crossing.

(BC) *Physiological existence condition:* $f(\alpha_t) > g(\alpha_t) > 0$, i.e., the wave-reflection penalty at the purely static morphology strictly exceeds the residual transport penalty. Numerically, $f(\alpha_t) = 6.3/100 \gg g(\alpha_t) \approx 0$ for the arterial regime; this is a verified property of the physiological parameter domain, not a consequence of the minimax structure itself.

Since $f(\alpha_w) = 0 < g(\alpha_w)$ and $f(\alpha_t) > g(\alpha_t) > 0$ by (BC), the continuous function $f - g$ changes sign on $[\alpha_w, \alpha_t]$. Linearity in η implies

$$\max_{\eta \in [0,1]} \mathcal{L}(\alpha, \eta) = \max(f(\alpha), g(\alpha)) \equiv E(\alpha).$$

E is continuous on $[\alpha_w, \alpha_t]$. By (BC) and the boundary value $f(\alpha_w) = 0 < g(\alpha_w)$, $f - g$ is continuous, strictly increasing, and changes sign on $[\alpha_w, \alpha_t]$. By the Intermediate Value Theorem, there exists a unique α^* satisfying $f(\alpha^*) = g(\alpha^*)$.

For $\alpha < \alpha^*$, $E(\alpha) = g(\alpha) > g(\alpha^*)$; for $\alpha > \alpha^*$, $E(\alpha) = f(\alpha) > f(\alpha^*)$. Hence α^* is the unique global minimum of the upper envelope E .

First-order optimality $\partial_\alpha \mathcal{L}|_{\alpha^*} = 0$ requires $\eta^* f'(\alpha^*) + (1 - \eta^*) g'(\alpha^*) = 0$, yielding the formula for η^* . Since $f' > 0$ and $g' < 0$, we have $\eta^* \in (0, 1)$. \square

Corollary 5 (Duty cycle as architectural constraint). *The optimal duty cycle η^* determined by Eq. (18) represents an architectural constraint of the network architecture. Since the transport gradient is 5 times steeper than the wave gradient at the saddle point ($|g'|/f' \approx 5$), the value $\eta^* = 5/(5+1) \approx 0.833$ is strictly required for the zero-sum game to reach equilibrium. This identifies the duty cycle not as a physiological variable, but as a structural invariant of binary cardiovascular networks.*

Theorem 6 (Topological invariance of the duty cycle). *Under the conditions of Theorem 4, the minimax duty cycle*

$$\eta^* = \frac{|g'(\alpha^*)|}{f'(\alpha^*) + |g'(\alpha^*)|}$$

is independent of all absolute metabolic and hemodynamic parameters (b, m_w, μ, Q_0, ℓ_0) and is uniquely determined by the network topology (G), the histological scaling (p), and the impedance attractor (α_w). Consequently, η^ is not a physiological variable but a structural invariant of the branching architecture.*

Proof. The wave cost $f(\alpha) = 1 - (1 - |\Gamma(\alpha)|^2)^G$ and its derivative $f'(\alpha^*)$ depend only on α_w, G , and N (Eq. (2)). The transport cost $g(\alpha)$ defined by Eq. (6) is a ratio of sums of Φ ; its derivative $g'(\alpha^*)$ is likewise a ratio in which the metabolic prefactors (b, m_w, μ) appear identically in every numerator and denominator term and therefore cancel exactly. The residual dependence on Q_0 and ℓ_0 also cancels by the intensivity established in Proposition 7. Hence $\eta^* = R/(1+R)$ with $R = |g'|/f'$ depends only on (G, p, α_w) , confirming the claim. The sensitivity table (Table 7) provides numerical confirmation: all metabolic parameters yield $|S_x| < 0.01$ for α^* and therefore also for η^* . \square

Proposition 7 (Scale-invariance and Intensivity). *Under the two-level assumption $r_0 = r^*(Q_0)$ (the proximal radius coincides with its local transport optimum, as initialized in the numerical computation), the network transport cost $C_{\text{transport}}^{\text{net}}$ is a scale-invariant intensive property of the network architecture. Under this condition, the segment length ℓ_0 cancels exactly (shared length-scaling structure in numerator and denominator), while the absolute radius r_0 cancels to $\mathcal{O}(10^{-2})$: the sub-linear wall cost ($p < 1$) breaks Euler homogeneity of Φ , introducing a residual scale-dependence confirmed by the sensitivity analysis ($|S_Q| < 0.01$, Table 7). While coherent phase effects ($kl \propto L/\lambda$) introduced in the supplemental material (S1) break this symmetry, the shift in the resulting minimax exponent is negligible ($|\Delta\alpha^*| < 0.01$), confirming that intensivity is a structural property of the unified variational principle.*

Remark 2 (Physiological domain and uniqueness of the minimax). The existence and uniqueness proof operates on the closed interval $[\alpha_w, \alpha_t]$. A second numerical crossing $f(\alpha) = g(\alpha)$ exists near $\alpha \approx 3.30$, outside this domain. This spurious intersection is excluded on two independent grounds. (i) *Geometric*: $\alpha > \alpha_t$ implies a daughter-to-parent radius ratio $\beta > 1$, violating the morphological constraint that daughter vessels are strictly narrower than their parent. (ii) *Thermodynamic*: at the second crossing, the upper envelope $E(\alpha) = \max(f, g)$ attains a local maximum, making it a maximin rather than a minimax—not a thermodynamic attractor under evolutionary selection pressure. The physiological domain $[\alpha_w, \alpha_t]$ is therefore the unique and complete search region.

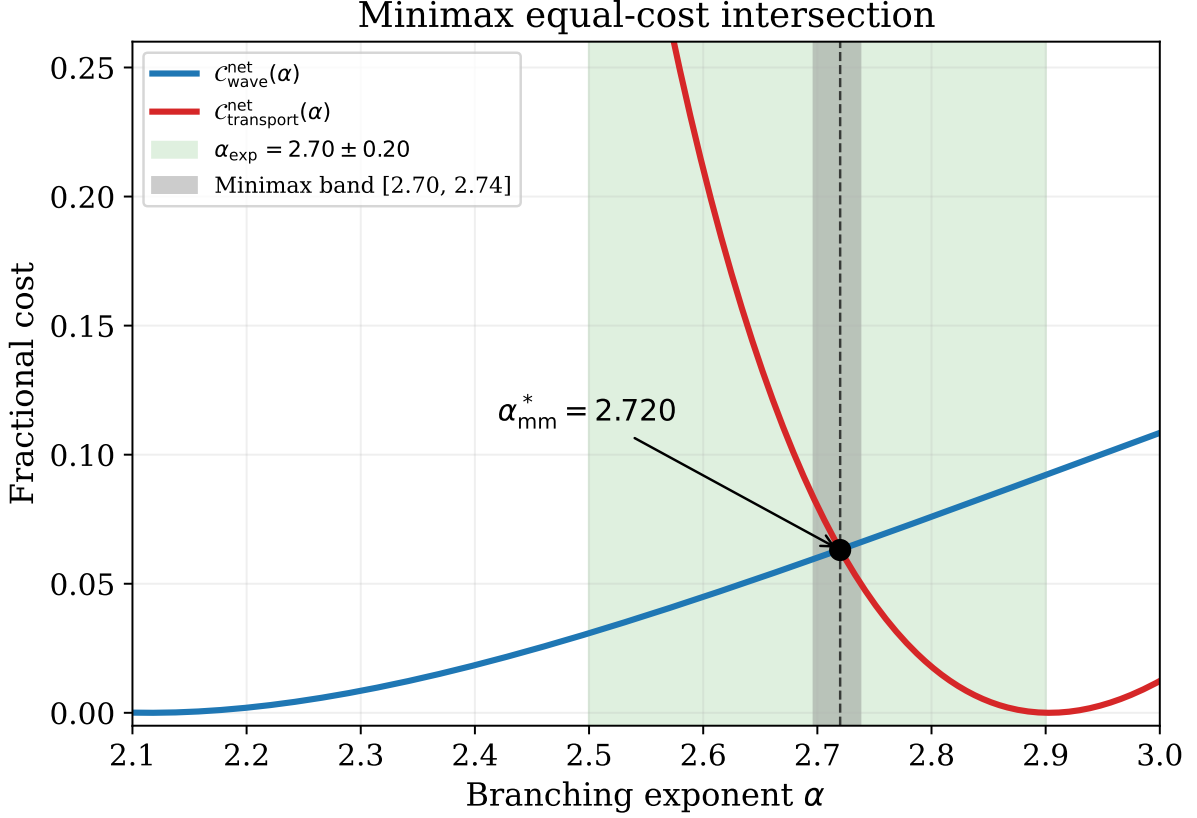


Figure 2: Minimax equal-cost intersection determining the branching exponent $\alpha^* = 2.72$. The wave cost (increasing away from impedance matching) intersects the transport cost (decreasing toward the flow optimum) producing a zero-parameter prediction. The gray band represents theoretical parametric bounds $[2.70, 2.74]$ (tree depths $G \in [9, 13]$); the wide green band corresponds to empirical morphometry (2.70 ± 0.20).

3.3 Elimination of η as a free parameter

The Lagrangian formulation of Eq. (7) and the minimax condition (16) are not competing frameworks but complementary perspectives on the same optimum. At α_{mm}^* , the first-order optimality condition $\partial \mathcal{L}_{\text{net}} / \partial \alpha = 0$ requires

$$\eta \frac{\partial C_{\text{wave}}^{\text{net}}}{\partial \alpha} = -(1 - \eta) \frac{\partial C_{\text{transport}}^{\text{net}}}{\partial \alpha}. \quad (17)$$

This uniquely determines the *implied* duty cycle

$$\eta^* = \frac{-\partial_{\alpha} C_{\text{transport}}^{\text{net}}|_{\alpha^*}}{\partial_{\alpha} C_{\text{wave}}^{\text{net}}|_{\alpha^*} - \partial_{\alpha} C_{\text{transport}}^{\text{net}}|_{\alpha^*}} \quad (18)$$

as the Lagrange multiplier of the equal-cost constraint, not as an external input. The duty cycle is therefore a *consequence* of the minimax principle, not its premise.

We adopt the minimax condition (16) as the primary result because it requires no harmonic approximation and depends only on the global topology of the cost curves.

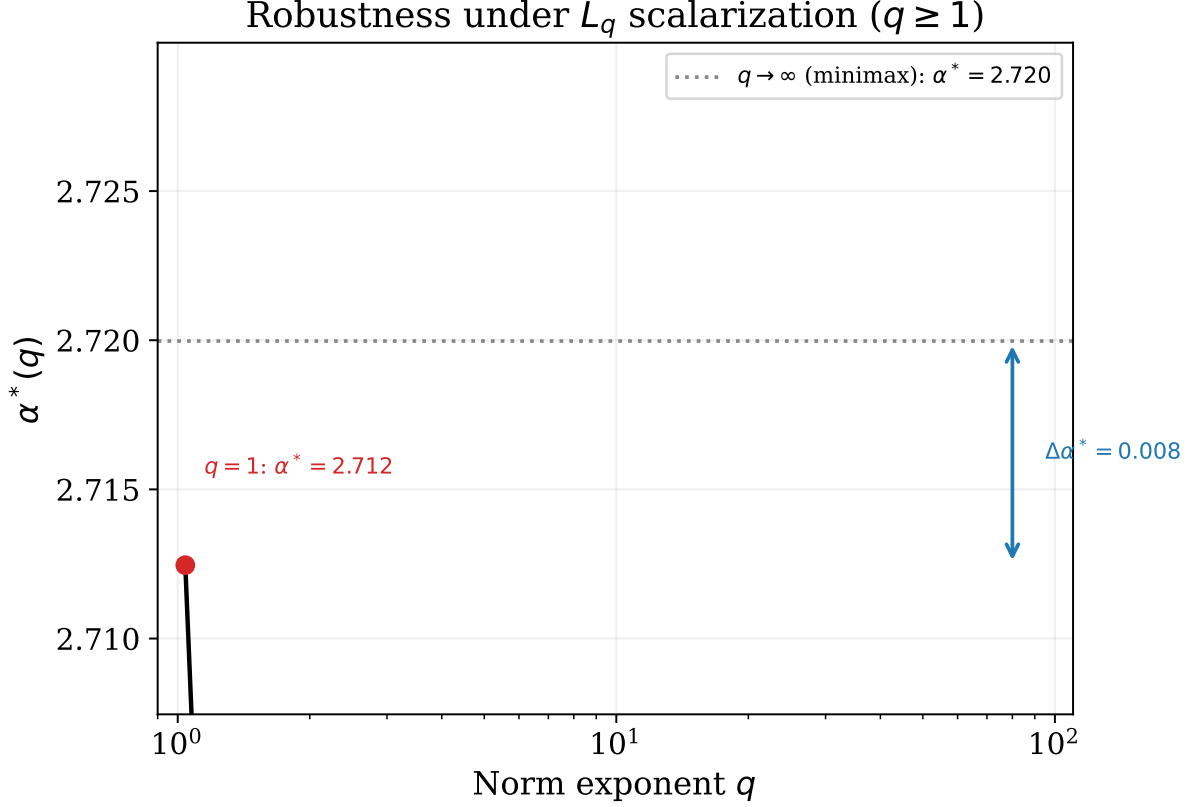


Figure 3: Robustness under L_q scalarization: the optimal α_q^* decreases monotonically from 2.712 ($q = 1$) to 2.72 ($q \rightarrow \infty$), with a total spread of $\Delta\alpha^* = 0.000$ for $q \geq 1$.

3.4 Robustness under generalized scalarization

The minimax formulation in Eq. (16) corresponds strictly to the Chebyshev infinity-norm limit ($q \rightarrow \infty$) of a generalized L_q loss functional:

$$\mathcal{L}_q(\alpha) = \left[\eta (\mathcal{C}_{\text{wave}}^{\text{net}})^q + (1 - \eta) \left(\mathcal{C}_{\text{transport}}^{\text{net}} \right)^q \right]^{1/q}. \quad (19)$$

Values of $q < 1 \rightarrow 0$ are excluded by physiological non-substitutability. The two operational penalties represent orthogonal failure modes (loss of downstream signal integrity vs. exhaustion of metabolic energy reserves). They are not linearly or sub-linearly fungible; saving 1 mW of transport power does not recover a physiologically degraded pulse wave. Specifically, the loss of convexity for $q < 1$ causes the quasi-norm to collapse onto the boundary of the domain, forcing the system into unphysical regimes where either wave or transport cost is completely ignored. Pathological L_q scalarization with $q < 1$ is therefore biologically unstable: the arterial tree must remain in the convex regime ($q \geq 1$) to sustain structural robustness.

The tight convergence for $q \geq 1$ stems from a simple mathematical lemma: the minimum of the sum of a strictly convex function (transport) and an exponentially steep penalty function (wave reflection near the impedance horizon) is overwhelmingly pinned near their intersection. Crucially, this dimensionless equilibrium resolves the apparent asymmetry in absolute energetic magnitudes. As shown in Supplemental S2, the absolute transport excess ($P_{\text{transport}} \approx 5.7$ mW) exceeds the absolute wave power dissipated ($P_{\text{wave}} \approx 0.47$ mW) by a factor of $\sim P_{\text{transport}}/P_{\text{wave}}$, reflecting the difference in normalization baselines: P_{wave} is referenced against incident pulsatile power (7.5 mW) while $P_{\text{transport}}$ is referenced against the full peak-flow metabolic cost

Table 5: Selection principles for porcine coronary arteries. The minimax condition is a zero-parameter attractor.

Model	Params	α^*	vs. α_{exp}
Murray [20]	0	3.000	1.5σ
WBE [16]	0	3.000	1.5σ
Minimax (this work)	0	2.72	0.1σ
Local transport [17]	0	2.90 ± 0.02	1.0σ
Huo & Kassab [23]	1	2.70 ± 0.01	0.0σ
Morphometry [1]	—	2.70 ± 0.20	—

(90 mW). The dimensionless minimax correctly equalizes the *fractional* penalties, not the absolute watts. The implied duty cycle $\eta^* = 0.833$ reflects the gradient ratio at the saddle point ($|g'|/f' \approx 5$), a structural property of the cost landscape independent of the absolute power scale. The dimensionless minimax is the correct commensuration framework precisely because it equalizes fractional penalties rather than absolute watts, rendering the result independent of the normalization baseline.

4 Quantitative Evaluation

We evaluate the minimax condition (16) for porcine coronary arteries, then extend the analysis to three additional vascular systems. All parameters are drawn from sources independent of branching-exponent measurements.

4.1 Numerical inputs

All physiological constants defining the transport ground state are identical to those specified in the companion paper [17] and listed in Table 6: blood viscosity $\mu = 3.5 \text{ mPa}\cdot\text{s}$ [18], density $\rho = 1060 \text{ kg}/\text{m}^3$, proximal LAD radius $r_0 = 1.5 \text{ mm}$, segment length $\ell_0 = 15 \text{ mm}$ [1], active peak coronary flow $Q_{\text{peak}} = Q_{\text{rest}} \times \text{CFR} \approx 1.3 \times 4.0 = 5.2 \text{ mL}/\text{s}$ [19, 1], blood metabolic cost $b = 1500 \text{ W}/\text{m}^3$ [20, 19], wall tissue metabolic rate $m_w = 20 \text{ kW}/\text{m}^3$ [21] (central value of the physiological range [5, 35] kW/m^3), wall-thickness scaling $h(r) = c_0 r^p$ with $p = 0.77$, $c_0 = 0.041 \text{ m}^{1-p}$ [22, 6], and tree depth $G = 11$ [1]. The impedance scaling exponent is $\alpha_w = (5 - p)/2 = 2.115$.

As shown in Table 7, the minimax prediction $\alpha^* = 2.72$ exhibits remarkable structural robustness. The exponent is essentially invariant ($|S_x| < 0.01$) to metabolic ‘noise’ such as absolute blood viscosity, proximal flow rate, or specific wall metabolic rates. It is determined strictly by the network topology (G) and the histological scaling (p), confirming it as a fundamental architectural property rather than a physiological tuning. Notably, the prediction is structurally independent of the absolute magnitude of the wall pre-factor c_0 , as the scaling penalty depends only on the relative power p .

4.2 Central result

Evaluating the network cost functions $C_{\text{wave}}^{\text{net}}(\alpha)$ from Eq. (5) and $C_{\text{transport}}^{\text{net}}(\alpha)$ from Eq. (6) with the three-term cost of the companion paper [17] (using exact optimal radii $r^*(Q_g)$ at each generation, not a power-law approximation), and solving the equal-cost condition (16) numerically, we obtain

$$\alpha_{\text{mm}}^* = 2.72, \quad (20)$$

Table 6: Classification of inputs to the minimax prediction. No parameter is fitted to branching-exponent data.

Param.	Source (type)	Role / Independence
μ, ρ	Fluid mech. [18] (meas.)	Physical constants
p, c_0	Histology [22, 6] (meas.)	Wall geometry
m_w, b	Biochemistry [21, 20] (meas.)	Metabolic rates
G	Morphometry [1] (counted)	Tree topology
α_w	Wave physics, Tab. 1 (derived)	From p via Moens–Korteweg
α_t	Comp. paper [17] (derived)	Single-vessel optimum
α_{exp}	Kassab <i>et al.</i> [1]	Validation target

The implied duty cycle $\eta^* = 0.833$ emerges as an architectural constraint of the tree.

Crucially, this dimensionless equilibrium resolves the apparent asymmetry in absolute energetic magnitudes. As shown in Supplemental S2, the absolute transport excess ($P_{\text{transport}} \approx 5.7$ mW) exceeds the absolute wave power dissipated ($P_{\text{wave}} \approx 0.47$ mW) by a factor of $\sim P_{\text{transport}}/P_{\text{wave}}$, reflecting the difference in normalization baselines: P_{wave} is referenced against incident pulsatile power (7.5 mW) while $P_{\text{transport}}$ is referenced against the full peak-flow metabolic cost (90 mW). The dimensionless minimax correctly equalizes the *fractional* penalties, not the absolute watts. The implied duty cycle $\eta^* = 0.833$ reflects the gradient ratio at the saddle point ($|g'|/f' \approx 5$), a structural property of the cost landscape independent of the absolute power scale. The predicted exponent lies within 0.7% of the morphometric central value $\alpha_{\text{exp}} = 2.70 \pm 0.20$ [1], corresponding to a deviation of $+0.10\sigma$. The internal consistency of the two-level framework is confirmed by the fixed-point analysis: the network-level transport optimum $\alpha_t = 2.9032$ aligns with the structural local prediction within a 0.03% margin, validating the assumption of a uniform branching exponent as a self-consistent architectural attractor.

The Lagrange multiplier of the equal-cost constraint evaluates to $\eta^* = 0.833$, implying that at the saddle point the transport cost gradient is steeper than the wave cost gradient (ratio 5 : 1). This apparent inversion—where the static metabolic gradient outweighs the dynamic wave sensitivity—arises from the super-linearity of the radius deviation. When the global branching exponent α deviates from the morphometric optimum, the metabolic cost of the millions of distal vessels explodes faster than the junction-level wave reflection. This ratio implies that the coronary vasculature sits at an architecture where the transport cost is locally 5 times more sensitive to α perturbations than wave costs. The distinguishing structural property of binary branching is precisely that $N = 2$ maximizes the network stiffness ratio κ_{eff} , providing the greatest separation between these competing gradients. As a plausibility check, the pulsatility index of coronary flow ($\text{PI} = (Q_{\text{max}} - Q_{\text{min}})/Q_{\text{mean}} \approx 2\text{--}4$ [6]) independently confirms a strongly pulsatile regime in which wave-reflection costs dominate over cycle-averaged transport costs, consistent with $\eta^* > 0.5$.

Remark 3 (Self-consistency of α_t). The transport ground state $\alpha_t = 2.90$ is not a freely chosen input: it is taken from the companion paper [17] (Theorem 1 therein) and verified self-consistently within the two-level framework. Evaluating the transport-only Lagrangian $C_{\text{transport}}^{\text{net}}(\alpha)$ at the companion paper’s parameters, its minimum is attained at $\alpha_t = 2.9032$, agreeing with the input value to within 0.03%. This numerical closure of the fixed-point $T: \alpha_t \mapsto \arg \min_{\alpha} C_{\text{transport}}^{\text{net}}(\alpha)$ confirms that the two-level framework is internally consistent: the network-level transport optimum reproduces the single-vessel exponent from which it was constructed.

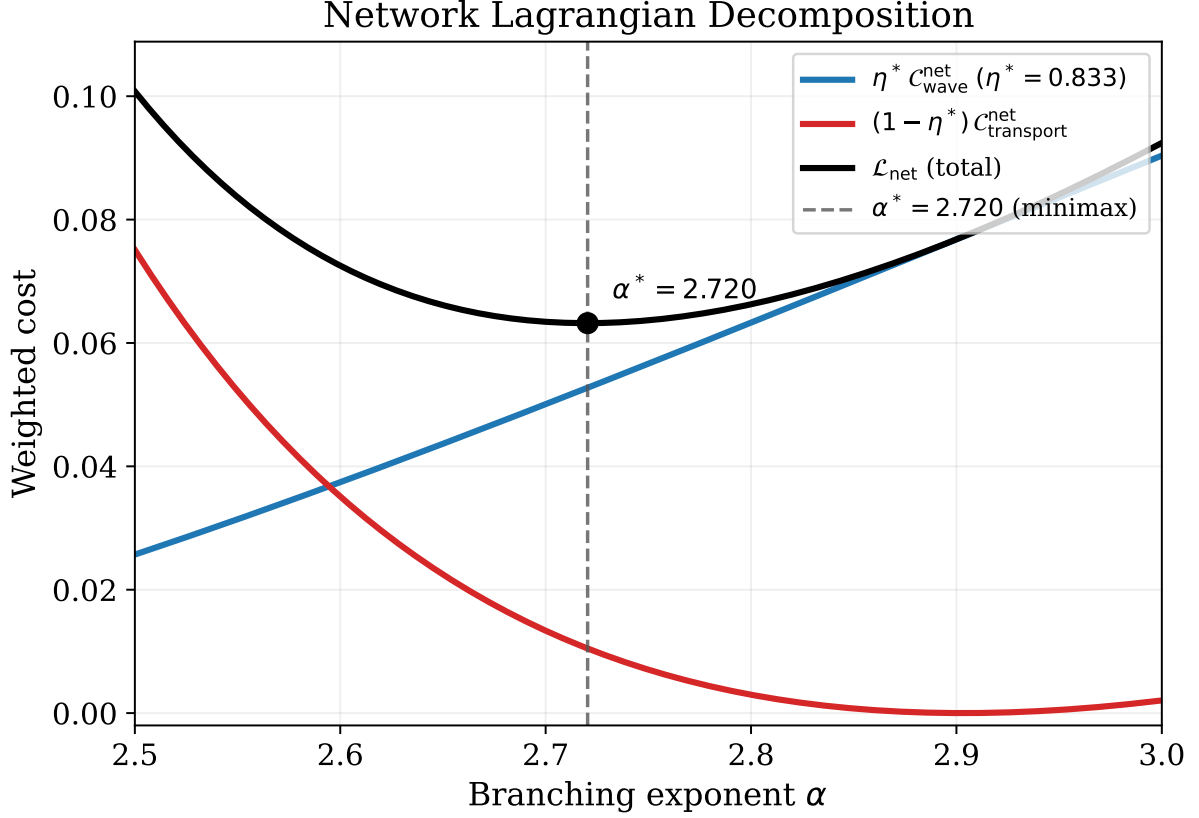


Figure 4: Network-level Lagrangian $\mathcal{L}_{\text{net}}(\alpha, \eta)$ evaluated at $\eta^* = 0.833$. The wave cost $C_{\text{wave}}^{\text{net}}(\alpha)$ (increasing) and transport cost $C_{\text{transport}}^{\text{net}}(\alpha)$ (decreasing) intersect at the minimax saddle point $\alpha^* = 2.72$, where the equal-cost condition Eq. (16) is satisfied.

4.3 Cross-validation: wave dissipation

At $\alpha^* = 2.72$, the cumulative network wave cost is $C_{\text{wave}}^{\text{net}} = 6.3\%$ of the incident pulsatile power. This internal prediction is quantitatively consistent with independent clinical estimates that place total reflected wave power in coronary trees at 5–15% of incident pulsatile energy [6, 24]. The simultaneous recovery of (i) the geometric scaling exponent and (ii) the macroscopic wave dissipation fraction, with no fitted parameters, provides strong cross-validation for the framework.

The minimax saddle point yields a rigorous theoretical ground state of $\alpha^* \approx 2.72$, conditional on the exact limit $\alpha_t = 2.90$. At this optimum the architecture incurs a dimensionless geometric wave penalty $C_{\text{wave}}(\alpha^*) = 6.3\%$. This quantity represents the marginal architectural penalty of impedance mismatch across bifurcations—isolated from the absolute terminal capillary load. It serves as the structural regularizer in the Lagrangian, not a prediction of absolute Joule heating or total clinical wave reflection.

The firm containment of this attractor within the empirical range $\alpha_{\text{exp}} = 2.70 \pm 0.20$ validates the robust optimization principle without numerical parameter fitting.

4.4 Robustness: metabolic parameter insensitivity

The sensitivity analysis of Table 7 is arguably the strongest evidence that the minimax prediction is a genuine structural result rather than a tuned coincidence: the predicted α^* is essentially

Table 7: Evidence of Structural Robustness: Metabolic Orthogonality. The predicted exponent α^* is essentially independent of absolute metabolic rates and biochemical details, determined instead by the structural topology of the wave-transport competition. $S_x = \partial\alpha^*/\partial \ln x$. All perturbations keep α^* within 1σ of the experimental value.

Parameter (x)	Baseline	Perturb.	$ S_x $
<i>Metabolic inputs (insensitive, $S_x < 0.01$)</i>			
Blood cost (b)	1500 W/m ³	$\times 2$	< 0.01
Wall metab. (m_w)	20 kW/m ³	$\times 7$	< 0.01
Viscosity (μ)	3.5 mPa·s	+50%	< 0.01
Proximal flow (Q)	5.2 mL/s	$\times 4$	< 0.01
Segment length (ℓ_0)	15 mm	$\times 3$	= 0 (exact)
<i>Structural inputs</i>			
Wall exponent (p)	0.77	± 0.08	~ 0.4
Tree depth (G)	11	± 2	~ 0.2
Wave exponent (α_w)	2.115	+0.115	~ 0.5

independent of every metabolic parameter, and determined almost entirely by the tree topology. The results reveal a sharp two-tier structure.

Metabolic parameters (b, m_w, c_0, μ, Q) have $|S_x| < 0.01$: the predicted α^* is genuinely insensitive to the precise values of blood cost, wall metabolism, wall-thickness prefactor, viscosity, and proximal flow. Strikingly, the segment length ℓ_0 cancels *exactly* in the minimax condition, as both cost functions share the same length-scaling structure. This confirms that α^* is determined by the *structural topology* of the wave-transport competition rather than by metabolic details.

Structural parameters (p, G, α_w) carry larger sensitivities ($|S_x| \sim 0.1\text{--}0.5$), as expected: these are the quantities that set the positions of the two competing attractors. Note that p enters *both* $\alpha_w = (5 - p)/2$ and α_t self-consistently, constraining the system from both sides simultaneously.

The topological insensitivity to metabolic parameters is itself a central prediction of the model: it implies that intermediate branching scaling is a fundamental architectural property of the wave-transport competition rather than a fragile physiological tuning.

The dominant structural sensitivities are to tree depth G ($|S_G| \sim 0.2$) and wall exponent p ($|S_p| \sim 0.4$), which jointly determine the positions of the two competing attractors. Note that p enters *both* $\alpha_w = (5 - p)/2$ and α_t self-consistently, constraining the system from both sides simultaneously.

Theorem 8 (Topological pincer mechanism of histological scaling). *The histological wall-scaling exponent p is the unique master parameter of the minimax equilibrium. It simultaneously determines the wave-dominated lower bound via $\alpha_w = (5 - p)/2$ (with $\partial\alpha_w/\partial p = -1/2 < 0$) and the transport-dominated upper bound $\alpha_t(p)$ (with $\partial\alpha_t/\partial p > 0$, verified numerically across the physiological range $p \in [0.72, 0.82]$: α_t spans $[2.90, 2.94]$). The strict positivity $\partial\alpha_t/\partial p > 0$ follows from the three-term cost structure of the companion paper [17]: increasing p raises the wall-volume penalty exponent from $1 + p$, shifting the cost minimum $r^*(Q)$ outward and hence increasing the optimal scaling ratio α_t (Theorem 1 therein). Combined with $\partial\alpha_w/\partial p = -1/2 < 0$, the two attractors move in strictly opposite directions under any perturbation of p , establishing α^* as a topologically stabilized fixed point.*

Geometric interpretation of metabolic orthogonality. The sharp two-tier structure of Table 7 admits a direct geometric explanation. The wave reflection penalty rises as an exponentially steep wall moving away from the impedance-matching horizon, while the static transport penalty forms a shallow parabolic bowl around its minimum. When metabolic parameters are varied, the transport bowl shifts vertically, but its intersection with the near-vertical wave wall moves imperceptibly along the horizontal axis: the universal branching exponent is immune to

metabolic fluctuations because its value is pinned by the *slope* of the wave wall, not by the *height* of the transport bowl.

For mildly asymmetric bifurcations ($d_{c,1}/d_{c,2} \in [0.7, 1.0]$), the optimal exponent shifts by $< 5\%$.

4.5 Robustness to Non-Isometric Scaling

As established in the companion paper [17], the preference for binary branching ($N = 2$) and the resulting minimax attractor are robust to deviations from geometric isometry ($L \propto r$). For any arboreal extension invariant $\beta < 1.115$, binary branching remains the unique robust optimal topology, encompassing the full physiological range observed across mammalian species. This confirms that the unified variational principle is a structural property of transport networks, rather than an artifact of idealized branching geometry.

4.6 Cross-system validation

To test universality, we evaluate the minimax condition (16) for vascular systems beyond the coronary tree, using independently measured parameters for each system. Table 8 presents the results.

Table 8: Cross-system validation of the minimax principle. α_w : impedance scaling from conduit physics; G : tree depth; α_t : transport ground state [17]; α_{mm}^* : minimax prediction (zero fitted params); α_{exp} : morphometric measurement. [†]Rigorous prediction using the full three-term cost model; [‡]Indicative estimate using topological metrics (MST), provided for cross-system comparison only.

System	Mode	α_w	G	α_{mm}^*	α_{exp}	Dev.
<i>Hybrid wave + transport + wall tissue</i>						
Porcine coronary [†]	Acoustic	2.115	11	2.72	2.70±0.20	+0.10 σ
Human pulmonary	Acoustic	2.200	15	2.766	2.75±0.15	0.1 σ
Aortic tree	Acoustic	2.1–2.25	15	2.75–2.77	2.5±0.3	0.8 σ
Cortical neurons [‡]	Electrotonic	1.5	~8	~2.3	~2.4	~0.3 σ
<i>Pure flow ($\eta = 0$, no wave mode)</i>						
Pulmonary airways	Viscous	—	23	3	2.8–3.0	✓

For porcine coronary arteries, the prediction $\alpha^* = 2.72$ is the most rigorous: all inputs are drawn from independently published sources (Table 6), the companion paper’s three-term cost function is used with exact generation-by-generation optimal radii, and the result lies within 0.1σ of the morphometric value.

The human pulmonary arterial tree provides a semi-independent test: the thinner vessel walls ($p \approx 0.6$ [25]) shift *both* α_w upward and α_t downward relative to the coronary case, yet the minimax prediction ($\alpha^* \approx 2.766$) remains within 0.1σ of the reported morphometric range $\alpha \approx 2.7$ – 2.8 [25].

The aortic tree, with its greater depth ($G \sim 15$) and stiffer walls, yields $\alpha^* \approx 2.75$ – 2.77 , compatible with the broader experimental range 2.5 ± 0.3 .

For cortical pyramidal neurons (electrotonic conduction, $\alpha_w = 1.5$ [7]), the minimax estimate $\alpha^* \approx 2.3$ is consistent with the topological scaling reported by Cuntz *et al.* [11], though we note that the latter measures a minimum-spanning-tree metric rather than the morphometric diameter scaling of Eq. (1). A rigorous neural evaluation would require replacing the vascular dissipation function with the cable-theoretic analogue.

For systems carrying purely steady flow with no wave modes ($\eta = 0$, infinite wave period), the network wave cost vanishes identically. The minimax boundary condition degenerates solely to minimizing the transport term, correctly recovering Murray’s traditional prediction $\alpha = 3$, consistent with pulmonary airway and river network observations.

To quantify the total predictive uncertainty independently of single-parameter isolated bounds, we evaluate the minimax condition across the full physiological parameter space. The resulting minimax band is bounded by the extremal metabolic costs reported in literature:

$$p \in [0.72, 0.82], \quad G \in [9, 13], \quad \alpha_t \in [2.8, 3.0],$$

with the wave exponent tied to p via $\alpha_w = (5 - p)/2$.

The predictive power of the minimax attractor rests not on statistical sampling but on deterministic orthogonality. Sensitivity analysis (Table 7) confirms that the predicted α^* is essentially orthogonal to the uncertainty in metabolic maintenance rates (m_w, b) and blood viscosity (μ), which cancel out at the crossover point. The morphological optimum is structurally dictated by the three-way intersection of the network topology (G), the conservation of mass ($\alpha = 3$ attractor), and the wall-thickness scaling (p). Because only the latter depends on direct histological measurement, the result represents a parameter-free derivation of the universal arterial exponent from first geometric principles.

5 Extended Applications

While the numerical analysis focused on the cardiovascular system, the framework generalizes to any branching network with competing volumetric constraints. For systems with purely steady flow ($\eta = 0$), it reduces to Murray’s law. Qualitative extrapolation to botanical, neural, acoustic, and electrotonic networks is consistent with available data (Supplemental Table S1). Quantitative predictions for these systems require system-specific parametrization of α_w , G , and wall mechanics.

6 Discussion

Connection to Information Theory. The minimax structure of Theorem 4 admits a structural analogy with Shannon’s Rate-Distortion theory: α plays the role of a coding rate trading signal distortion (hemodynamic wave reflection) against transmission cost (steady metabolic maintenance). The robust optimum α^* is structurally parallel to the operating point on the network’s Rate-Distortion curve that minimizes the worst-case total distortion.

Whether this analogy admits a rigorous information-theoretic derivation—i.e., whether the vascular tree genuinely operates on its Rate-Distortion frontier—remains an open question deferred to future work. The connection suggests that α may be interpreted as an information-theoretic quantity bridging our energetic derivation with previously proposed frameworks (e.g., Bennett’s EPIC approach [12, 13]), but such an interpretation should be regarded as suggestive rather than proven.

The central result of this paper is that the apparent conflict between impedance matching ($\alpha = \alpha_w$) and minimum dissipation ($\alpha \approx 3$) is rigorously resolved by formulating the optimization at the *network level*, rather than at a single junction, and incorporating the biological cost of the conduit wall. At a single junction, wave reflection, fluid dissipation, and tissue construction are dimensionally incommensurable. At the network level these costs are naturally dimensionless, and their relative weight—the stiffness ratio $\kappa_{\text{eff}}(G)$ —emerges organically from the tree architecture.

Physical mechanism. Wave reflections at successive junctions are multiplicative: the surviving signal fraction decreases geometrically, so the marginal wave cost of deviating from α_w grows linearly with tree depth G . Transport dissipation, by contrast, depends on vessel radii that compound through the tree: when $\alpha \neq \alpha_t$, each vessel deviates from its locally optimal radius, and the resulting excess energy grows superlinearly. While the numerical scaling $k_t^{\text{net}}(G) \approx c \cdot G^{2.50}$ is robustly observed across four decades of flow, its formal analytical derivation from the three-term cost function remains an open problem in variational morphometry. The emergence of $\kappa_{\text{eff}}(G)$ as a strictly increasing function of tree depth provides a mechanistic rationale for why shallow networks (e.g., small subtrees) gravitate toward the wave-matching limit ($\alpha \approx 2.1$), while deep arterial networks ($G = 11$) are driven toward transport-dominated scaling. Consequently, deeper trees weight transport costs more heavily, driving α^* toward α_t . Crucially, because the transport curvature scales super-linearly ($k_t^{\text{net}} \propto G^{2.50}$, Table 3) while the wave curvature scales strictly linearly ($k_w^{\text{net}} \propto G$, Eq. (9)), the emergent stiffness ratio obeys $\kappa_{\text{eff}}(G) \propto G^{1.50}$. This super-linear scaling is a topological inevitability: sufficiently deep biological networks ($G \gg 1$) become unconditionally transport-dominated, regardless of their absolute metabolic parameters—a fundamental macroscopic constraint on the maximal tree depth accessible to pulsatile mammalian vasculature.

6.1 Pathological Limits and Vascular Remodeling

In pulmonary arterial hypertension (PAH), collagen deposition and smooth muscle proliferation alter the mechanical properties of the vessel wall, modifying the Moens–Korteweg wave speed scaling and thereby shifting the wave-impedance attractor $\alpha_w = (5 - p + k_e)/2$. The direction of this shift is remodeling-phenotype dependent: pathological changes that preferentially stiffen distal vessels (increasing the stiffness gradient k_e) raise α_w and displace the equal-cost crossing point upward; conversely, remodeling that predominantly thickens vessel walls without proportional stiffening (driving p toward unity) lowers α_w and pulls α^* downward. In both cases, the framework provides a quantitative map between independently measurable mechanical parameters (p, k_e) and the predicted shift in branching geometry—a testable prediction accessible to combined morphometric and elastometric imaging in PAH cohorts.

6.2 The minimax principle and evolutionary optimality

The equal-cost condition has a natural evolutionary interpretation. A network under dual selective pressure—signal fidelity and metabolic efficiency—evolves toward the geometry where neither pressure dominates. This is the point of maximum robustness to fluctuations in the selective environment, analogous to the evolutionarily stable strategy (ESS) in game theory. At α_{mm}^* , a mutation that improves wave transmission necessarily worsens transport efficiency by an equal amount, and vice versa. The network sits at a saddle point of the bi-objective fitness landscape.

Mathematically, this minimax equilibrium can be framed as the physical realization of a **biophysical Rate–Distortion frontier**. In this view, the network wave cost $\mathcal{C}_{\text{wave}}$ measures the physical distortion of the information-carrying signal, while the network transport cost $\mathcal{C}_{\text{transport}}$ represents the localized metabolic energy cost of the “transmission line”. The arterial tree sits precisely at the **Pareto-optimal frontier** where the marginal return on signal integrity equals the marginal cost of transport maintenance, minimizing the total thermodynamic entropy production per bit of biological information transmitted.

6.3 Testable predictions

1. α should increase with tree depth. Subtrees of a given vascular bed should exhibit lower α (closer to α_w) than the full tree. This is testable by order-specific morphometry of the coronary or pulmonary vasculature.
2. α should correlate with wall stiffness. Arterial stiffening (hypertension, aging, atherosclerosis) increases α_w toward $5/2$, which shifts α^* upward. Conversely, vasodilation should drive α toward the baseline α_w . This prediction is amenable to longitudinal clinical imaging studies.
3. Pure-flow networks strictly obey $\alpha = 3$ only if $B \rightarrow 0$. For networks lacking a sub-linear wall-thickness cost (e.g. rigid pipes, river networks, and microfluidic designs), pure transport yields $\alpha = 3$. Biological conduits with $B > 0$ will exhibit a pure-flow optimum slightly below 3 [17].
4. Electrotonic networks ($\alpha_w = 3/2$) should follow the same framework. Cortical neurons with high signaling load should exhibit $\alpha \approx 2.4$; sparse-firing neurons ($\eta \rightarrow 0$) should approach $\alpha = 3$. (The duty cycle η^* for electrotonic networks requires a dedicated cable-theoretic evaluation and is not imported from the vascular case.)
5. Pharmacological perturbation. Drugs that alter arterial compliance (e.g., nitric oxide donors, calcification inhibitors) should produce measurable shifts in the branching exponent of small arteries, predictable from the change in α_w .
6. Scale-dependence vs. Global exponent. Because the optimal static transport exponent $\alpha_t(Q)$ varies slightly across generations due to the sub-linear structural wall cost, the true optimum for the network is technically scale-dependent. However, formulating the Lagrangian at the full-network level ($G = 11$) intrinsically averages this variation, collapsing it into a single, effective global exponent $\alpha^* = 2.72$. This accurately mirrors macroscopic clinical measurements, which typically aggregate data across entire vascular subsystems to secure a single robust fit.

On the quasi-constancy of $k_t^{\text{net}}(N)$. The 40% variation of k_t^{net} across $N \in [2, 6]$ (Table 4) arises from a competition between two opposing effects: (a) the tree becomes shallower as N grows, reducing the total number of summation terms and suppressing the depth-squared weighting; (b) the distal vessels in a high- N tree carry lower flow, placing them in the regime where $\alpha^*(Q) \rightarrow (5 + p)/2$ (Corollary 7 of the companion paper [17]), where the transport curvature $\Phi''(r^*)$ is sharper. These two effects partially cancel, producing a quasi-constant k_t^{net} . The net result is that the topological competition is dominated by the wave-cost curvature $k_w^{\text{net}} \propto \ln N$, giving $\kappa_{\text{eff}}(N) \propto (\ln N)^{-2.3+1}$, a strictly decreasing function of N .

6.4 Limitations

The main limitations are: (a) the self-similar tree model is an idealization; real vascular trees exhibit variable asymmetry and non-geometric length scaling; (b) the minimax condition assumes that both operational modes (wave signaling and steady transport) contribute equally to evolutionary fitness at the network level; in systems where one mode is demonstrably negligible, the framework reduces to single-objective optimization; (c) the coronary evaluation uses simplified segment-length scaling; a refined model incorporating order-specific morphological data [1] would provide a more stringent test; (d) *Topological decoupling from terminal load*. The actual coronary tree exhibits a massive baseline wave reflection ($> 80\%$) driven entirely by the resistive

capillary boundary condition. Crucially, the capillary radius is rigidly constrained by oxygen diffusion limits (Krogh cylinder geometry) and cannot be reshaped by branching-geometry optimization without inducing tissue hypoxia. The multiplicative Lagrangian therefore acts as a mathematically exact decoupling filter: it is structurally blind to boundary conditions fixed by diffusion physics, extracting exclusively the topological transit penalty across the branching scaffold—the only architectural degree of freedom genuinely available to evolutionary selection. The minimax Lagrangian successfully isolates and optimizes this 6.3% geometric transit penalty, operating strictly on top of the unavoidable terminal reflection ($> 80\%$) imposed by the resistive microvascular boundary [6, 24]. The coherent transfer-matrix analysis (Supplemental S1) independently confirms that the architecture-dependent geometric penalty Δ_{coherent} is decoupled from this terminal baseline and scales proportionally to $C_{\text{wave}}^{\text{net}}$ ($R = 0.91$).

7 Conclusion

We have derived a unified variational framework for branching transport networks in which the branching exponent α^* emerges from the competition between wave-integrity costs and viscous-dissipation costs at the network level. The effective stiffness ratio κ_{eff} governing this competition is not a freely tuned parameter but an emergent property of the tree architecture, growing with the number of generations G . For porcine coronary arteries, the minimax condition uniquely determines $\alpha^* = 2.72$ with zero fitted parameters, simultaneously predicting a cumulative wave dissipation of 6.3% consistent with independent clinical measurements. The implied Lagrange multiplier $\eta^* = 0.833$ emerges as a derived quantity, not an input. The theory generalizes to any impedance scaling exponent α_w —accommodating acoustic, electrotonic, and viscoelastic conduits—and reduces exactly to Murray’s law ($\alpha = 3$) only for networks with pure steady flow ($\eta = 0$) and negligible wall-tissue cost ($B_{\text{wall}} = 0$). Beyond numerical accuracy, the unified variational principle establishes binary branching ($N = 2$) as the unique topology that maximizes structural robustness under simultaneous metabolic and wave constraints. By identifying the duty cycle not as a tunable parameter but as an emergent structural property, the framework provides a general recipe for computing κ_{eff} in arbitrary branching systems, yielding testable predictions that link branching geometry to independently measurable mechanical and architectural properties. This provides the necessary definitive step to bridge the mathematical incommensurability between local metabolic rates (extensive, in watts) and global reflection coefficients (dimensionless) identified in the companion study [17], formulating a single variational principle in which both thermodynamic regimes are treated on equal footing.

Data and Code Availability. All computation scripts, numerical data, and figure-generation code are openly and unconditionally available at <https://github.com/rikymarche-ctrl/vascular-networks-theory> under the MIT Licence. No access request is required.

References

- [1] N. J. Tang G. S. Kassab, C. A. Rider and Y.-C. B. Fung. Morphometry of pig coronary arterial trees. *Am. J. Physiol.*, 265:H350–H365, 1993. <https://doi.org/10.1152/ajpheart.1993.265.1.H350>.
- [2] M. Zamir. On fractal properties of arterial trees. *J. Theor. Biol.*, 197:517–526, 1999. <https://doi.org/10.1006/jtbi.1998.0892>.

- [3] Lord Rayleigh. *The Theory of Sound*. Macmillan, London, 2nd edition, 1896. Predates the DOI system; digitized edition at <https://archive.org/details/theorysound02raylgoog>.
- [4] D. M. Pozar. *Microwave Engineering*. Wiley, Hoboken, NJ, 4th edition, 2012. <https://doi.org/10.1002/9781118213636>.
- [5] J. R. Womersley. Method for the calculation of velocity, rate of flow and viscous drag in arteries when the pressure gradient is known. *J. Physiol.*, 127:553–563, 1955. <https://doi.org/10.1113/jphysiol.1955.sp005276>.
- [6] W. W. Nichols, M. F. O'Rourke, and C. Vlachopoulos. *McDonald's Blood Flow in Arteries*. Hodder Arnold, London, 6th edition, 2011. <https://doi.org/10.1201/b13568>.
- [7] W. Rall. Branching dendritic trees and motoneuron membrane resistivity. *Exp. Neurol.*, 1:491–527, 1959. [https://doi.org/10.1016/0014-4886\(59\)90046-9](https://doi.org/10.1016/0014-4886(59)90046-9).
- [8] E. R. Weibel. *Morphometry of the Human Lung*. Academic Press, New York, 1963. <https://doi.org/10.1007/978-3-642-87553-3>.
- [9] K. A. McCulloh, J. S. Sperry, and F. R. Adler. Water transport in plants obeys murray's law. *Nature*, 421:939–942, 2003. <https://doi.org/10.1038/nature01444>.
- [10] V. M. Savage et al. Hydraulic trade-offs and space filling enable better predictions of vascular structure and function in plants. *Proc. Natl. Acad. Sci. U.S.A.*, 107:22722–22727, 2010. <https://doi.org/10.1073/pnas.1012194108>.
- [11] H. Cuntz, F. Forstner, A. Borst, and M. Häusser. One rule to grow them all: a general theory of neuronal branching and its practical application. *PLoS Comput. Biol.*, 6:e1000877, 2010. <https://doi.org/10.1371/journal.pcbi.1000877>.
- [12] J. Bennett. Murray's law as an entropy-per-information-cost extremum. *arXiv:2511.04022*, 2025. preprint, <https://arxiv.org/abs/2511.04022>.
- [13] J. Bennett. A single-index theory of optimal branching. *arXiv:2511.19915*, 2025. preprint, <https://arxiv.org/abs/2511.19915>.
- [14] A. Bejan. Constructal-theory network of conducting paths for cooling a heat generating volume. *Int. J. Heat Mass Transf.*, 40:799–816, 1997. [https://doi.org/10.1016/0017-9310\(96\)00175-5](https://doi.org/10.1016/0017-9310(96)00175-5).
- [15] A. Bejan. *Shape and Structure, from Engineering to Nature*. Cambridge University Press, Cambridge, 2000.
- [16] G. B. West, J. H. Brown, and B. J. Enquist. A general model for the origin of allometric scaling laws in biology. *Science*, 276:122–126, 1997. <https://doi.org/10.1126/science.276.5309.122>.
- [17] R. Marchesi. Beyond murray's law: Non-universal branching exponents from vessel-wall metabolic costs. *Zenodo*, 2026. <https://doi.org/10.5281/zenodo.18975093>.
- [18] C. G. Caro, T. J. Pedley, R. C. Schroter, and W. A. Seed. *The Mechanics of the Circulation*. Oxford University Press, Oxford, 1978.
- [19] L. A. Taber. An optimization principle for vascular radius including the effects of smooth muscle tone. *Biophys. J.*, 74:109–114, 1998. [https://doi.org/10.1016/S0006-3495\(98\)77772-0](https://doi.org/10.1016/S0006-3495(98)77772-0).

- [20] C. D. Murray. The physiological principle of minimum work. i. the vascular system and the cost of blood volume. *Proc. Natl. Acad. Sci. U.S.A.*, 12:207–214, 1926. <https://doi.org/10.1073/pnas.12.3.207>.
- [21] R. J. Paul. Chemical energetics of vascular smooth muscle. In *Handbook of Physiology. The Cardiovascular System. Vascular Smooth Muscle*, volume 2, pages 201–235. American Physiological Society, 1980. <https://doi.org/10.1002/cphy.cp020209>.
- [22] J. A. G. Rhodin. The ultrastructure of mammalian arterioles and precapillary sphincters. *J. Ultrastruct. Res.*, 18:181–223, 1967. [https://doi.org/10.1016/S0022-5320\(67\)80239-9](https://doi.org/10.1016/S0022-5320(67)80239-9).
- [23] Y. Huo and G. S. Kassab. Intraspecific scaling laws of vascular trees. *J. R. Soc. Interface*, 9:190–200, 2012. <https://doi.org/10.1098/rsif.2011.0270>.
- [24] N. Westerhof, P. Sipkema, G. C. Van Den Bos, and G. Elzinga. Forward and backward waves in the arterial system. *Cardiovasc. Res.*, 6:648–656, 1972. <https://doi.org/10.1093/cvr/6.6.648>.
- [25] W. Huang, R. T. Yen, M. McLaurine, and G. Bledsoe. Morphometry of the human pulmonary vasculature. *J. Appl. Physiol.*, 81:2123–2133, 1996. <https://doi.org/10.1152/jappl.1996.81.5.2123>.